Fuel 319 (2022) 123734

Contents lists available at ScienceDirect

Fuel

journal homepage: www.elsevier.com/locate/fuel

Full length article

Fuel efficiency optimisation based on boosting control of the particulate filter active regeneration at high driving altitude

Pedro Piqueras [a,*], Richard Burke [b], Enrique José Sanchis [a], Bárbara Diesel [a]

[a] CMT-Motores Térmicos, Universitat Politècnica de València, Camino de Vera s/n, 46022 Valencia, Spain
[b] University of Bath, Claverton Down, Bath, BA2 7AY, UK

ARTICLE INFO

Keywords:
Internal combustion engine
Particulate filter
Altitude
Soot oxidation
Thermal management
Regeneration

ABSTRACT

The air pressure change as a function of the driving altitude affects negatively the engine performance and emissions as well as the efficiency of the exhaust aftertreatment systems (ATS). These detrimental effects have driven the emissions standards to account for the altitude as boundary condition in type-approval tests. The new requirements demand to balance the recovery of the engine performance as the altitude increases by means of control strategies avoiding negative effects on tailpipe emissions, i.e. combination of engine-out emissions and ATS performance. In this context, this study identifies experimentally the need of optimisation of the active regeneration strategies applied to wall-flow particulate filters for altitude driving. Firstly, a particulate filter was subjected to active regenerations at altitudes ranging from sea-level to 2500 m for a variety of initial soot loads. As boundaries, the engine worked according to the series calibration, which was found to be a function of the altitude for the boosting system actuation. The results evidenced a noticeable deterioration of the soot oxidation rate as the altitude increased. In fact, some operating conditions showed an early balance between filtration and oxidation that avoided the completeness of the regeneration process. The root causes of the soot depletion rate reduction, which involved thermal and transport phenomena, are reasoned from the combined analysis of experimental and modelling approaches. The conclusions provided a guide to successfully conduct the turbine actuation for an optimum exhaust thermal management during the regeneration event at altitude.

1. Introduction

The European energy policies for air quality protection has led to the inclusion of type-approval real driving emission (RDE) tests [1] for passenger car and light duty vehicles that must take into account the ambient temperature and driving altitude as boundary conditions. While Euro 6d accounts for sea-level to 1300 m and −7 to 35°C [2] as ranges for the extended ambient conditions, different limits are defined worldwide according to the characteristics of every country. Thus, warmer ambient conditions are considered in India (8–45°C) or higher upper limit for altitude (2400 m) are imposed in Chinese regulations.

The altitude variation, which involves different ambient pressure, has been already studied in terms of effects on the combustion [3] and gas exchange processes [4], as well as the aftertreatment systems (ATS) performance [5]. Different studies in heavy duty engines have reported a penalty in specific fuel consumption [6], especially as the vehicle speed increases [7]. The fuel consumption deterioration has been also observed in passenger car diesel engines operating at high altitude, again with a progressive penalty from urban [4] to extra-urban driving conditions [8]. Regarding pollutants, NO_x emission tend to increase as altitude does [8]. In particular, the exhaust gas recirculation (EGR) rate is decreased as the engine load increases to keep the compressor surge margin while the turbine inlet temperature and turbocharger speed limits are prevented [4]. Consequently, these strategies result in a relevant penalty in NO_x emission [9]. Along with the NO_x emission penalty, Wang et al. [10] also showed the increase of CO and particulate matter (PM) in tests performed up to 3000 m, in agreement with Serrano et al. till 2500 m [4]. These effects were governed by the oxygen shortage promoting the formation of soot precursors [11].

The increase of the PM emissions and the lower O_2 availability harms the particulate filter (PF) response [12] in altitude operation compared to the sea-level case. The direct consequence is the delay of the balance point between filtration and passive regeneration [13] due to the need of high soot loads to produce the increase of the oxidation rate. As a result, the exhaust back-pressure tends to increase. The consequences are penalties in engine performance and the need of more frequent active regeneration events, which adversely affect the fuel economy [14] and engine-out emissions [15,16]. Regarding the dynamics of active regenerations in altitude, an additional concern can

* Corresponding author.
E-mail address: pedpicab@mot.upv.es (P. Piqueras).

https://doi.org/10.1016/j.fuel.2022.123734
Received 14 December 2021; Received in revised form 4 February 2022; Accepted 27 February 2022
Available online 15 March 2022

Definitions/Abbreviations

A_f	filtration area in the control volume
c_{gas}	gas flow molar concentration
c_p	specific heat
E_a	activation energy
E_{PI}	efficiency of the post-injection strategy
$H_{f,k}$	enthalpy of formation of species k
k_n	kinetic constant of the oxidation reaction with reactant n
K_{S_n}	adsorption equilibrium constant
$\dot{m}$	mass flow
m_s	soot mass
$m_{s,reg}$	regenerated soot mass
M	molar mass of chemical species
n_n	moles of reactant n
p	pressure
p_n	partial pressure of reactant n
P_f	pre-exponential factor
P_S	adsorption pre-exponential factor
$\dot{q}_{reg}$	power released by soot oxidation
S_p	soot specific surface
t	time
T	temperature
u_w	filtration velocity
X	molar fraction
z	tangential dimension

Acronyms

ATS	aftertreatment system
BSFC	brake specific fuel consumption
CA aTDC	crank angle degree after top dead centre
DOC	diesel oxidation catalyst
DPF	wall-flow diesel particulate filter
ECU	engine control unit
EGR	exhaust gas recirculation
HP	high pressure
HSDI	high-speed direct injection
LHV	lower heating value
LP	low pressure
MEDAS	multifunctional efficient dynamic altitude simulator
MTM	MEDAS temperature module
PF	particulate filter
PM	particulate matter
RDE	real driving emission
SCR	selective catalytic reduction
SCRf	selective catalytic reduction filter
SOI	start of injection
VGT	variable geometry turbine

Greek letters

α	completeness index
δ	partial derivative
Δ	variation
ΔH_S	adsorption enthalpy
η_{int}	internal pore diffusion efficiency
ν	stoichiometric coefficient
θ	surface coverage

Subscripts

C	Carbon
exh	exhaust
ext	external
f	fuel
in	inlet
int	internal
k	gaseous species
max	maximum
n	gaseous reactant
pl	particulate layer
PI	post-injection
reg	regeneration
$regular$	engine regular mode
s	soot
w	porous wall

appear related to the PF inlet temperature. A common actuation when operating at altitude consists of closing the variable geometry turbine (VGT) to increase the boosting pressure and compensate the reduction in ambient density with respect to sea-level [17]. Consequently, the higher turbine expansion ratio involves a greater decrease on temperature across the turbine. Despite the effect of VGT closing on the turbine inlet temperature, this strategy tends to decrease the aftertreatment inlet temperature [18]. Nevertheless, the final response during the active regeneration also depends on a complex interaction with the post-injection strategy [19]. In this regard, the objective is to maximise the efficiency of the post-injection process, i.e. to make the post-injected fuel to increase the PF inlet temperature being directly burned out in the oxidation catalyst. Although this process is traditionally set up by means of the post-injected fuel amount and the post-injection angle [20], the air management also plays a key role.

In parallel to the engine actuation, the variation of the PF boundary conditions as a function of the altitude affects the regeneration process. The soot oxidation mechanism involves the reactant diffusion, adsorption and, finally, reaction [21]. The reaction kinetics depends simultaneously and non-linearly on the temperature [22], the concentration of the reactants [23] and the intrinsic soot properties [24]. In this regard, the dependence of the soot depletion rate on the reactant concentration and the selectivity of the oxidation process has been widely explored in the literature [25] and key aspects of the regeneration analysis by modelling tools [26]. On the one hand, some studies assume that the reaction rate has a linear relationship with the oxidant concentration for Diesel soot [27] and soot from other sources [28]. This approach has been proved valid within a limited range of temperatures and compositions. Studies carried out in broader ranges have shown that this dependence is not really linear [29] and shows different behaviour as a function of the soot source and O_2 concentration [30]. Along with the soot reactivity dependence on the reactant concentration for modelling proposals, the composition of the reaction products has been also discussed [31]. This way, models accounting for the CO selectivity during soot oxidation has been proposed [32], usually in the form completeness index of the oxidation reaction [33].

In this work, the impact of series calibrated active regeneration strategies on the soot oxidation dynamics of a diesel PF was evaluated as a function of the driving altitude. Sea-level, 1300 m and 2500 m were considered along with different thresholds in soot load to trigger the regeneration event. The experiments were carried out in a Euro 6d-Temp passenger car Diesel engine coupled to an altitude

Table 1
Main specifications of the engine.

Engine type	HSDI Diesel
Emissions standards	Euro 6d-Temp
Number of cylinders	4 in line
Displaced volume [cm^3]	1461
Stroke [mm]	80.5
Bore [mm]	76
Number of valves	2 per cylinder
Compression ratio	15.2:1
Rated power @ speed	81 kW @ 4000 rpm
Rated torque @ speed	260 Nm @ 1750 rpm
Fuel Injection	Common-rail direct injection
Turbocharger	VGT
EGR	HP-and cooled LP-EGR
ATS	Closed-coupled DOC+DPF

Table 2
Main DOC and DPF geometric parameters.

	DOC	DPF
Monolith diameter [mm]	120	170
Monolith length [mm]	140	80
Channel cross-section	Square	Square
Cell density [cpsi]	400	400
Cell size [mm]	1.04	0.95
Wall thickness [mm]	0.23	0.32
Catalytic area [m^2]	3.95	
Filtration area [m^2]		2.1
Porosity [–]		0.40
Mean pore diameter [μm]		20.4
Permeability [$\times 10^{13}$ m^2]		7.59

simulator Horiba MEDAS [34,35]. Next, the regeneration process was reproduced computationally by a one-dimensional compressible flow solver for wall-flow PFs including the diffusion and adsorption of the reactants [26]. The experimental results evidenced the reduction of the soot depletion rate as the altitude increased. In most cases, the balance point was reached early leading to a high soot mass remaining within the filter. The reasons for the deterioration of the regeneration dynamics are discussed disclosing thermal from mass transfer and O_2 adsorption effects. From this analysis, the potential of the boosting strategy in altitude to bring soot oxidation benefits was explored. Besides the recovery of the soot depletion rate to sea-level values, the engine efficiency and emissions during the regeneration processes were also improved with respect to series calibration.

2. Experimental setup

The study was carried out in a series production Euro 6d-Temp Diesel passenger car engine. The main characteristics of the engine are summarised in Table 1. With respect to air management, the engine was equipped with a VGT, water charge air cooler as well as high pressure (HP) and water cooled low pressure (LP) EGR. The aftertreatment system was composed of a close-coupled diesel oxidation catalyst (DOC) followed by a wall-flow diesel PF (DPF) coated as selective catalytic reduction (SCRf). Nevertheless, the urea injection and the series underfloor selective catalytic reduction (SCR) system were omitted in this work. The geometry of the DOC and DPF is described in Table 2.

As sketched in Fig. 1, the engine crankshaft was connected to an asynchronous dynamometer controlled by the automation system AVL PUMA Open to set the engine torque and speed. The air supply was handled by an altitude simulator coupled to the engine intake, exhaust and sump to impose and control the required ambient boundary conditions [36,37]. In particular, Horiba MEDAS, which was developed at CMT-Motores Térmicos [34,35] in partnership with Horiba Europe GmbH, was used. It was coupled to the extension MEDAS temperature module (MTM) providing precise pressure and temperature emulation capabilities within sea-level to 5000 m between −15 and 45°C.

Table 3
DPF pressure drop and soot mass load at the beginning of the regeneration events.

Pressure drop [mbar]	Soot load [g/l]		
	Sea-level	1300 m	2500 m
80	3.75	3.65	3.32
120	7.23	7.05	6.63
175	10.03	9.71	9.06
230	13.12	12.82	12.03

The engine hardware accounted for an open engine control unit (ECU) whose calibration was accessed through ETAS INCA software. In particular, the LP-EGR rate and the post-injection strategy set in series calibration were kept, coinciding in all altitudes. Opposite, the VGT position was variable with altitude. In a final step, its actuation was modified with respect to the series calibration in order to optimise the soot oxidation rate, what is forward described in Section 4.

The engine and aftertreatment system responses were monitored during the tests. The engine torque and speed were registered by the dynamometer and the in-cylinder pressure was measured by glow-plug piezoelectric pressure transducer Kistler 6055B. The air mass flow was measured by the on-board mass flow sensor whilst the fuel mass flow was obtained by an AVL 733S gravimetric balance together with a temperature and pressure control device AVL-753, ending up by reaching the common-rail. The complete fuel line is illustrated in the upper part of Fig. 1. The fuel mass flow repartition according the injection pattern was obtained from the ECU. The flow path along the engine intake and exhaust systems, including the inlet and outlet of the DPF, was instrumented with K-type thermocouples and piezoresistive pressure sensors.

The gaseous emissions were monitored with a Horiba Mexa ONE gas analyser measuring upstream and downstream of the exhaust aftertreatment brick. Besides the engine out CO_2 emission, a gas sample from the intake manifold was also taken to measure the CO_2 molar fraction in that location and determine the EGR rate. Only LP-EGR rate was applied during the tests since HP-EGR was only considered during warm-up conditions. The O_2 molar fraction was measured by a lambda sensor placed between the DOC and the DPF. Lastly, the engine-out opacity was measured with an AVL 439 Opacimeter placed upstream of the DPF as well.

2.1. Test campaign

The active regeneration events were performed in the engine test bench varying the altitude and the DPF pressure drop at the beginning of the regeneration to account for the case sensitivity effect of different engine operating conditions and DPF boundaries. Sea-level, 1300 m and 2500 m were considered. The thresholds of pressure drop to trigger the active regeneration and their corresponding soot load as a function of the altitude are listed in Table 3. The trends in soot load showed a decrease with altitude for the same pressure drop, which was mainly caused by the exhaust density reduction according to the ambient one. Assuming constant exhaust mass flow, the reduction of the gas density as the altitude increases produces the velocity increase. As described by Payri et al. [38], it makes Darcy's pressure drop increase because of its linear dependence on the filtration velocity. In addition, the pressure drop also increases across the DPF due to the inertial contributions due to these depend squarely on the velocity and linearly on the density. Therefore, since the regenerations were triggered at the same pressure drop at all altitudes, the soot load was expected to decrease as the altitude increased to offset the density impact. Nevertheless, the specific soot load corresponding to every tested condition was also determined by the exhaust mass flow and temperature, which were not the same at all altitudes. These flow conditions also affected the gas velocity, density, and Darcy's pressure drop in the particulate layer and, hence, set the resulting soot load.

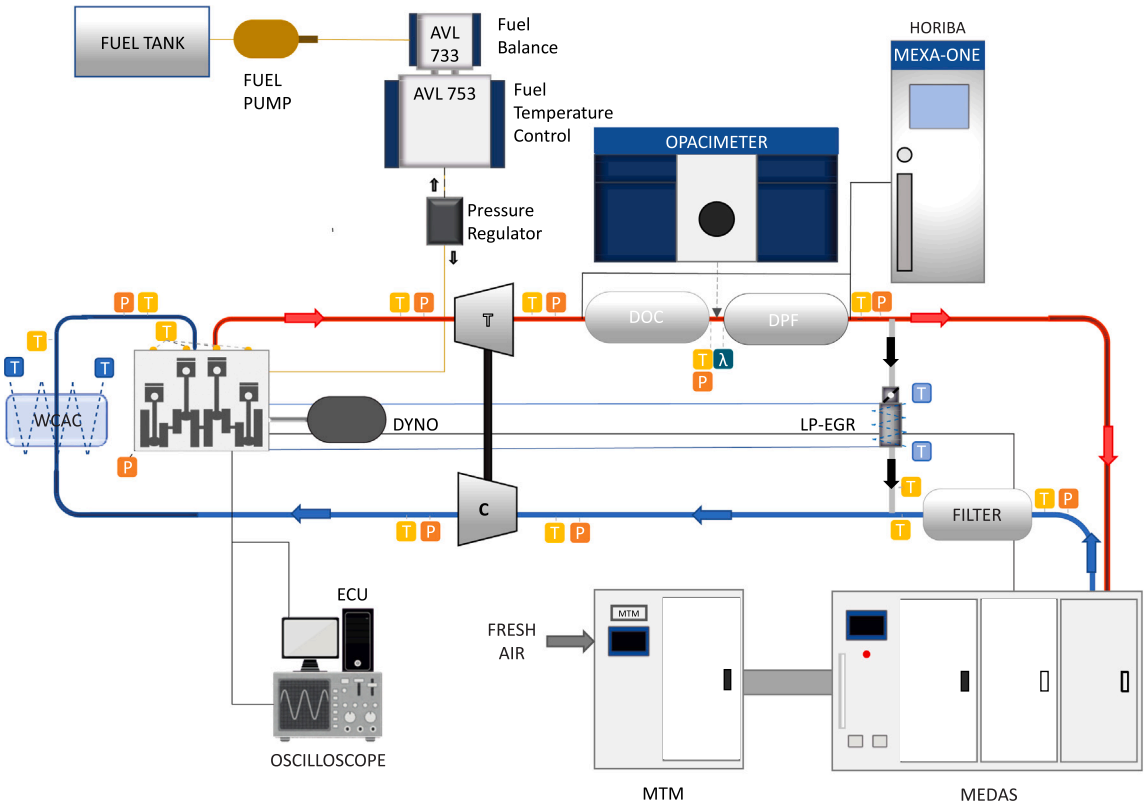

Fig. 1. Scheme of the engine test cell.

The engine was run at 2000 rpm and constant pedal (37%) along every regeneration event. Although a constant torque approach would have been representative of the driver's behaviour, the resulting operating conditions would have been different between regular and regeneration modes, initial pressure drop for regeneration and, among the different altitudes considered in the study. This strategy would have led to 24 operating points with the same engine speed but a different pedal. Consequently, the analysis would have been much more complex because the engine actuation would have been affected by the case and calibration of each different point. Probably it would have avoided clarifying some key hints on the limitations that can arise during DPF regeneration in altitude, as discussed in the following sections. By contrast, constant engine speed and pedal, and hence fuel at every engine mode (Table 4), for all operating points means that the resulting engine response was due to combustion mode, altitude and, DPF pressure drop threshold, i.e., due to the differences in calibration of the parameters that define the study.

The injection profile and the in-cylinder pressure corresponding to the sea-level case with 175 mbar as DPF pressure drop are depicted in Fig. 2(a) for regular mode, i.e. prior to trigger the active regeneration strategy. The fuel mass per injection event is listed in Table 4. Two pilot injections close to the main one can be identified, mainly used to control emissions and noise, and a post-injection with the aim to reduce, specially, NO_x emissions [39]. The regeneration mode was activated once the target DPF pressure drop was reached applying the series ECU calibration. The injection profile during the active regeneration events and the in-cylinder pressure corresponding to sea-level case are represented in Fig. 2(b). The total injected fuel mass was increased from 18.25 mg/cc to 26.32 mg/cc during the active regenerations. Along this mode, the two pilot injections were also advanced to increase the premixed combustion phase whilst the main injection was delayed increasing its amount of fuel according to Table 4. In addition to the fuel quantity increase in the post-injection, this was split into two events to minimise oil dilution. The first post-injection was delayed with respect to the regular mode while the second one was placed at the very end of the expansion stroke aiming to prevent its combustion into the cylinder, thus promoting the oxidation of the unburned HCs in the DOC and take advantage of the subsequent DPF inlet temperature increase [40].

Table 4
Fuel injection profile in regular and regeneration modes at 2000 rpm and pedal 37%.

Injection	Regular mode		Regeneration mode	
	SOI [CA aTDC]	Mass [mg/cc]	Angle [CA aTDC]	Mass [mg/cc]
Pilot 1	−8.9	1.52	−14.3	1.2
Pilot 2	−2.9	1.27	−4.7	1.29
Main	2.5	13.57	7.3	17.03
Post 1	15.1	1.89	44	3.42
Post 2	–	–	140	3.38
Total		**18.25**		**26.32**

Besides the change of the injection profile when triggering the regeneration, the LP-EGR rate and VGT position were also modified during this operating mode. The impact of the control actuation on these parameters is analysed in Section 4.

3. PF regeneration model

The PF regeneration model [26] applied in this study to analyse the impact of the engine operation at variable altitude was implemented into a thermo-and fluid dynamic single-channel lumped solver for wall-flow monoliths [41], which integrated the modelling of pressure drop [42], heat transfer [43], soot filtration and meso-and micro-geometry variation in the wall-flow monolith [44].

The model accounts for the soot oxidation in the presence of O_2 and NO_2 [45],

$$C + \alpha_{O_2} O_2 \rightarrow 2(\alpha_{O_2} - 0.5)CO_2 + 2(1 - \alpha_{O_2})CO \quad (1)$$

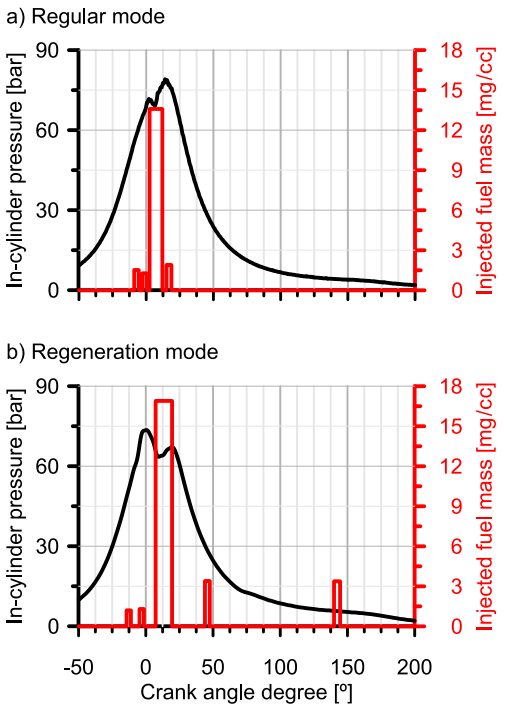

Fig. 2. Fuel injection profile and in-cylinder pressure in (a) regular and (b) regeneration modes at 2000 rpm and pedal at 37%.

$$C + \alpha_{NO_2} NO_2 \rightarrow \alpha_{NO_2} NO + (2 - \alpha_{NO_2})CO + (\alpha_{NO_2} - 1)CO_2 \quad (2)$$

where α_n stands for the oxidation completeness index of the reactant n according to the proposal of Jeguirim et al. [46]. Assuming the regeneration as a quasi-steady process [47], the one-dimensional conservation equation of the reactant species across every porous medium (particulate layer and ceramic substrate) is then written as [26]:

$$u_w \frac{\partial p_n}{\partial z} = -\left(S_{p,ext} + \eta_{int_n} S_{p,int}\right) \alpha_n k_n \theta_n, \quad (3)$$

In Eq. (3), $S_{p,ext}$ represents the external soot specific surface, $S_{p,int}$ accounts for the internal one and η_{int_n} is the internal pore diffusion efficiency of reactant n as a way to consider the effective specific surface of the soot particles [26]. Besides, the reaction rate is proportional to the soot oxidation kinetic constant (k_n), which is calculated according to the Arrhenius expression [48], and the gas reactant surface coverage (θ_n) defined by the Langmuir isotherm,

$$\theta_n = \frac{K_{S_n} p_n}{1 + K_{S_n} p_n}, \quad (4)$$

which has been proved to provide a good estimate of the surface concentration of NO_2 [49] and O_2 [26]. In particular, the Langmuir isotherm provides good results in O_2 excess conditions, whilst the Dubinin–Radushkevich isotherm captures better the soot oxidation dynamics for very low O_2 concentration [30]. Thus, the surface coverage in Eq. (4) represents the reaction dependence on the reactant partial pressure (p_n) and the substrate temperature (T_w) by means of the adsorption equilibrium constant (K_{S_n}).

Eq. (3) is solved applying a 4th-order Runge–Kutta method in the particulate layer and the porous substrate. The mole variation of each reactant (O_2 and NO_2) at each layer of the porous medium is obtained from the solution of the reactant transport equation as

$$\frac{\partial n_n}{\partial t} = X_n u_w A_f c_{gas} \quad (5)$$

where c_{gas} is the gas flow molar concentration. The soot oxidation rate is finally determined from the O_2 and NO_2 depletion rates

$$\frac{\partial m_{s,reg}}{\partial t} = M_C \left(-\frac{1}{\alpha_{NO_2}} \frac{\partial n_{NO_2}}{\partial t} - \frac{1}{\alpha_{O_2}} \frac{\partial n_{O_2}}{\partial t} \right), \quad (6)$$

where M_C is the carbon molecular weight. Finally, the heat power released during the soot oxidation process in every layer of the porous medium is determined considering the gaseous reactants depletion rate and the enthalpy of formation ($H_{f,k}$) of the involved species in each soot oxidation reaction:

$$\dot{q}_{reg} = \sum_n \dot{q}_{reg,n} = \sum_n \sum_k \frac{\nu_{k,n}}{\alpha_n} H_{f,k} \frac{\partial n_n}{\partial t} \quad (7)$$

4. Discussion of the results

Fig. 3 shows the change in VGT position and LP-EGR rate from regular to regeneration mode cases applying series ECU calibration in plots (a) and (b), respectively. A variety of altitudes and DPF pressure drops at the beginning of the active regeneration events were considered. Being 100% the fully closed position, the VGT was gradually closed as the altitude increased, as observed in Fig. 3(a). During the active regeneration, the results showed a tendency of VGT opening but highly dependent on the altitude. The VGT position was opened from 74% to 49% at sea-level case when the regeneration was triggered. However, this variation was lower at 1300 m and, finally, the VGT was kept fully closed at 2500 m. The differences in LP-EGR rate before and during regeneration were also narrowed as a function of the altitude. In regular operation, the ECU decreased the LP-EGR rate as the altitude increased from 30% at sea-level to 12% at 2500 m. However, during active regeneration events, it was kept constant at 9%, regardless the DPF mass load and driving altitude.

As shown in Fig. 3(c), the air mass flow during regular operation increased with altitude as a consequence of the VGT and LP-EGR control. The objective was to avoid the engine torque derating [5]. Fig. 3(d) shows the boost pressure change with altitude. It was kept within a narrow range for regular operation regardless the altitude, i.e. the ambient pressure decrease was compensated by the pressure ratio increase due to the closer VGT position. In addition, the boost pressure in regular mode showed sensitivity to the DPF pressure drop, whose increase penalised the boost pressure. By contrast, the boost pressure was higher in regeneration mode than regular one as well as increasing with altitude due to the closer VGT position and higher VGT inlet temperature, as shown in Fig. 4(a). This strategy made the fresh air mass flow to remain constant in regeneration mode regardless the altitude. Hence, the equivalence ratio also remained constant (iso-fuel tests), as well as the exhaust mass flow since the LP-EGR rate was also kept constant with altitude in regeneration mode (Fig. 3(b)). Consequently, the exhaust gas residence time across the DPF during the regenerations was exclusively dependent on the exhaust gas density as a function of the altitude, as forward discussed.

Concerning torque and brake specific fuel consumption (BSFC), their complementary variations with altitude are observed in Figs. 3(e) and (f), respectively. As already evidenced in boost pressure, more sensitivity to the DPF pressure drop was reflected on engine performance deterioration as altitude increased. The same trends as in regular mode were obtained during the active regeneration processes for torque and BSFC. The torque increased during the regeneration mode with respect to regular operation because of the opener VGT and LP-EGR rate decrease and even despite the constant air mass flow boundary with altitude. However, the new torque did not compensate the fuel mass increase related to the active regeneration strategy. As a result and the BSFC was increased, with further penalisation in altitude operation.

Fig. 4 shows additional exhaust flow properties. As suggested by the VGT trend with altitude, both VGT inlet temperature and pressure increased in regular and regeneration modes, as presented in Figs. 4(a) and (b). Nevertheless, further sensitivity was observed in regeneration

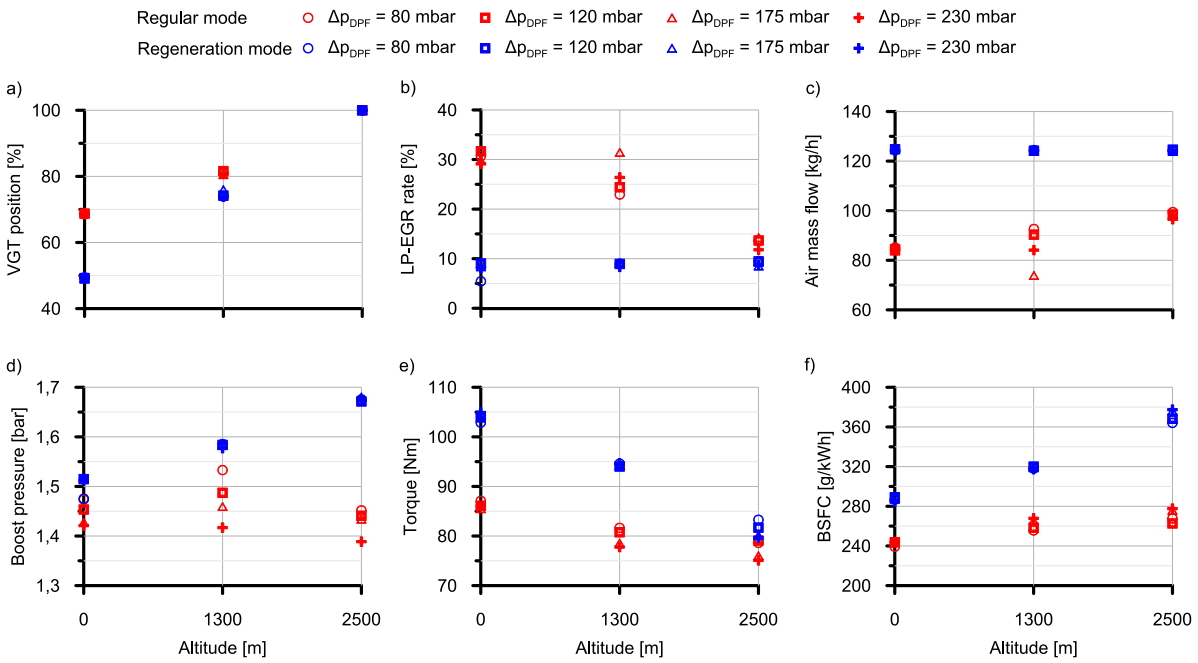

Fig. 3. Actuation on VGT and LP-EGR due to active regeneration strategy and effects on engine performance, air mass flow and boost pressure as a function of altitude and initial DPF pressure drop.

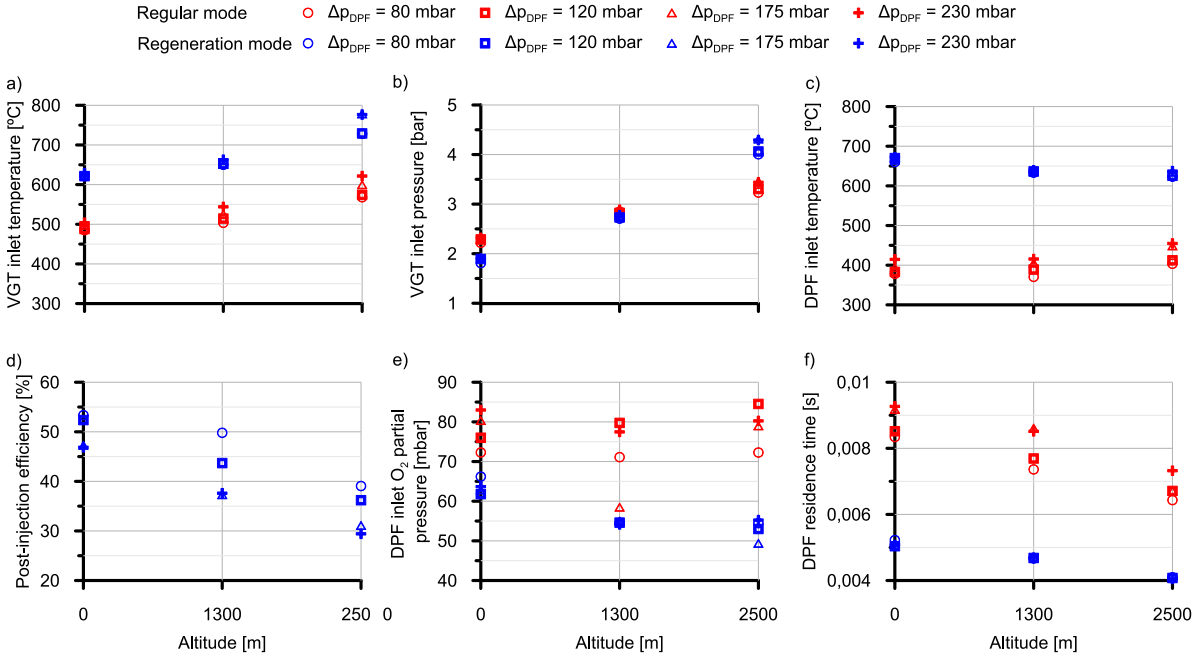

Fig. 4. Exhaust flow properties at VGT and DPF inlet, fuel post-injection efficiency, DPF inlet O_2 partial pressure and DPF residence time as a function of the engine operation mode, altitude and initial DPF pressure drop.

mode due to the injection setup. Therefore, higher temperature and pressure were found at the VGT inlet during regeneration mode that in regular one, with increasing differences as the altitude increased. The very high VGT inlet pressure caused an increase in the BSFC due to the increased pumping work, despite of the boost pressure increase.

As regards to the DPF, the regeneration strategy produced a relevant increase of the gas inlet temperature with respect to the regular mode, but with decreasing benefit as the altitude increased, as represented in Fig. 4(c). Despite the higher VGT inlet temperature with altitude, the also higher VGT expansion ratio (higher VGT inlet pressure and lower DPF inlet pressure with altitude) along with low VGT efficiency related to the very closed position produced a temperature drop that limited the DPF inlet temperature. The temperature gain due to the activation of the regeneration strategy dropped from 275°C at sea level (675°C in DPF inlet temperature) to 175°C (625°C in DPF inlet temperature) at 2500 m. This trend indicates a deterioration of the efficiency of the post-injection strategy as the altitude increased. The variation of this parameter, which is computed in temperature terms according to Eq. (8) [20], is shown in Fig. 4(d).

$$E_{PI} = \frac{T_{DPF,in} - T_{DPF,in_{regular}}}{T_{DPF,in_{max}} - T_{DPF,in_{regular}}}, \tag{8}$$

The post-injection efficiency is computed from the actual temperature at the DPF inlet during the regeneration ($T_{DPF,in}$,), the DPF inlet temperature before the regeneration strategy is triggered ($T_{DPF,in_{regular}}$) and the maximum temperature that might be reached at the DPF inlet if all post-injected fuel was oxidised adiabatically within the DOC assuming constant the regular exhaust mass flow ($T_{DPF,in_{max}}$):

$$T_{DPF,in_{max}} = T_{DPF,in_{regular}} + \frac{\dot{m}_{f,PI} LHV}{\dot{m}_{exh_{regular}} c_p} \quad (9)$$

In addition to the lower DPF inlet temperature as the altitude increased, the O_2 partial pressure at the DPF inlet and the residence time also played a role in the effective soot oxidation rate. Figs. 4(e) and (f) represent these variables as a function of the altitude. The equivalence ratio reduction in regular operation as altitude increased allowed the O_2 partial pressure to be kept in similar levels at all altitudes, offsetting the ambient pressure decrease. However, the O_2 partial pressure was clearly reduced during the regeneration process, being this trend more important as the altitude increased due to the ambient pressure reduction while keeping constant the equivalence ratio. Likewise the DPF inlet temperature, this tendency contributed to the soot oxidation rate decrease as the altitude increased. A similar conclusion is obtained from the analysis of the residence time. On the one hand, it decreased at constant altitude during the regeneration mode because of the higher temperature and exhaust mass flow than in regular mode. On the other hand, the decrease of ambient pressure as the altitude increased did not compensate the slightly lower DPF inlet temperature and made the residence time, which is shown in Fig. 4(f), lower during the regeneration and minimum at 2500 m.

According to these boundary conditions, the evolution of the DPF pressure drop along several regeneration cases is represented in Fig. 5. The extreme thresholds of DPF pressure drop to trigger the regeneration mode, i.e. 80 and 230 mbar, are shown at each column comparing experimental and modelled DPF pressure drop and outlet temperature for the three studied altitudes. Regarding the model setup, Table 5 lists the pre-exponential factors and activation energies to calculate the Arrhenius kinetic constants for soot oxidation. These were calibrated from the complete set of experiments for the case of O_2 but imposed from previous literature data obtained by the authors for NO_2 [26]. Although the calibration of soot oxidation by NO_2 came from a different DPF and engine, this decision was taken because of the negligible impact of NO_2 on the total soot oxidation rate during active regenerations, which O_2 governs. This is due to the O_2 contribution itself, especially compared to the low NO_2 concentration because of the low NOx emission and the high temperature (equilibrium NO_2/NOx ratio was assumed at the outlet of the DOC, i.e., the most favouring conditions for NO_2). Therefore, calibrating the NO_2 kinetic constants exclusively based on active regeneration would have led to a low-accurate result. Nevertheless, the authors checked that the soot oxidation entirely depleted the NO_2 with the proposed kinetic constants, thus confirming the negligible impact on the results that lower NO_2 activation energy would have had. Finally, it is also interesting to highlight that the regeneration model described in Section 3 accounts for two stages before the chemical reaction: the diffusion of the reagents (O_2/NO_2) within the soot particles and their adsorption on the surface. As explained by Macián et al. [26], to account explicitly for these stages leads to the increase of the apparent activation energy of the reaction. It justifies that these values fall into the upper range of typical values found in the literature [50].

Additionally, Table 5 provides the adsorption equilibrium constant parameters, i.e. the adsorption enthalpy (ΔH_{S_n}), which is defined as the adsorption to desorption activation energy difference, and the adsorption pre-exponential factor (P_{S_n}). Finally, the external and internal soot specific surfaces used in this work [26] are also detailed.

Fig. 5 shows in plots (a) and (b) very good agreement between experimental and modelled pressure drop during the regeneration process as a function of altitude, especially for the lowest initial DPF pressure drop cases (80 mbar). Nonetheless, the trends at 230 mbar were also captured accurately despite predicting a lower pressure drop reduction rate at sea-level conditions. The ability of the model to reproduce the soot oxidation was also evidenced in the prediction of the DPF outlet gas temperature, which is represented in Figs. 5(c) and (d). Again, the main deviations appeared at the 230 mbar case for sea-level conditions, where the temperature peak appearing during the maximum reactivity phase was smoothed by the underestimated oxidation rate. In fact, these deviations are related to the model dependence on the lumped estimate of the wall temperature, which averaged the local thermal gradients along the monolith [26].

Table 5
Soot oxidation kinetic parameters in DPF model.

P_f [m $\frac{\text{bar}}{\text{s}}$]	O_2	27
	NO_2	6
E_a [J/mol]	O_2	1.2×10^5
	NO_2	9.5×10^4
P_{S_n} [bar^{-1}]	O_2	1×10^{-4} [51]
	NO_2	5×10^{-5} [49]
ΔH_{S_n} [J/mol]	O_2	-7.7×10^4 [52]
	NO_2	-7.5×10^4 [53]
$S_{p,ext,pl}$ [m^{-1}]		6.72×10^7
$S_{p,ext,w}$ [m^{-1}]		3.67×10^6
$S_{p,int,pl}$ [m^{-1}]		1.897×10^8
$S_{p,int,w}$ [m^{-1}]		1.039×10^7

As regards the regeneration behaviour, the rate of reduction of the pressure drop suffered a significant decrease as the altitude increased, as outlined from the analysis of the flow properties at the DPF inlet during the regeneration process. The pressure drop is directly related to the soot depletion rate, which is represented in Fig. 6 along with its cumulative soot oxidised mass. The low soot loading case (80 mbar in initial pressure drop) was the most affected one by the altitude. The peak soot depletion rate reached 13.9 mg/s at sea-level operation for this soot loading condition, whilst it was reduced to 6.9 mg/s at 1300 m and dropped to ~ 4 mg/s at 2500 m. In addition, the soot depletion rate became very flat along time for these altitude cases. An earlier balance point was reached as the altitude increased as a consequence of the low reactivity in the described conditions.

By contrast, the higher soot depletion rate reached as the soot mass load increased, what is observed comparing plots (a) and (b) in Fig. 6, contributed to delay the balance point. In fact, increasing the soot mass load to trigger the active regeneration almost allowed the completeness of the oxidation process at 1300 m, as observed in Fig. 5(b). The results from Fig. 6 also highlight another relevant feature of these regeneration processes. The peaks of soot depletion rate for the maximum soot load (initial pressure drop of 230 mbar) shown in Fig. 6(b), i.e., 99.4 mg/s, 49.4 mg/s and 27.4 mg/s at sea-level, 1300 m and 2500 m, respectively, kept the same altitude-to-altitude ratio as for 80 mbar cases (Fig. 6(a)). This means that the maximum reactivity phases were kinetically controlled for all the pressure drop thresholds and altitudes. On the one hand, the maximum depletion rate was not high enough, even in sea-level cases, to make the mass transfer phenomena limit the reaction rate. On the other hand, these results also underline that the reduction of the residence time as the altitude increased, which was previously shown in Fig. 4(f), did not condition the regeneration response. This is a positive result for real life since the regeneration optimisation in altitude from state-of-the-art calibrations is limited to a thermal problem primarily.

In this regard, the lack of mass transfer limitations can be also understood as constant oxygen surface coverage across the particulate layer, as discussed next. Firstly, Fig. 7 presents the oxygen surface coverage as a function of the substrate temperature and the O_2 partial pressure computed according to the Langmuir isotherm (Eq. (4)). The specific oxygen surface coverage for the regeneration processes corresponding to 80 mbar in initial DPF pressure drop are also depicted in

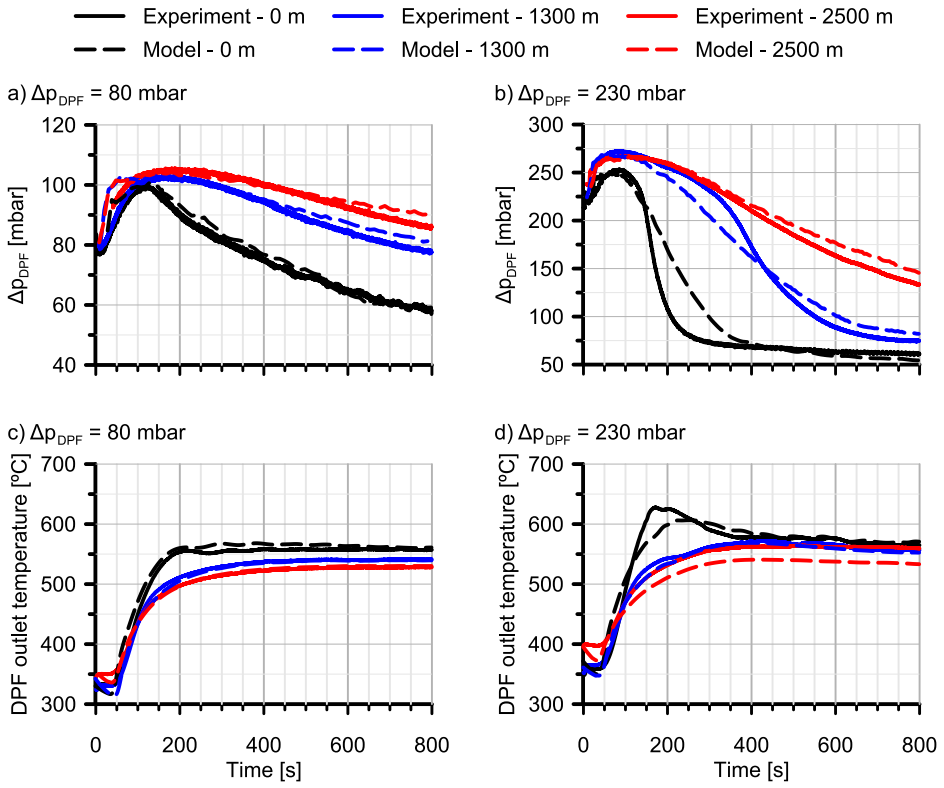

Fig. 5. Experimental and modelled DPF pressure drop and outlet gas temperature as a function of the altitude during active regeneration processes with initial DPF pressure drop 80 and 230 mbar.

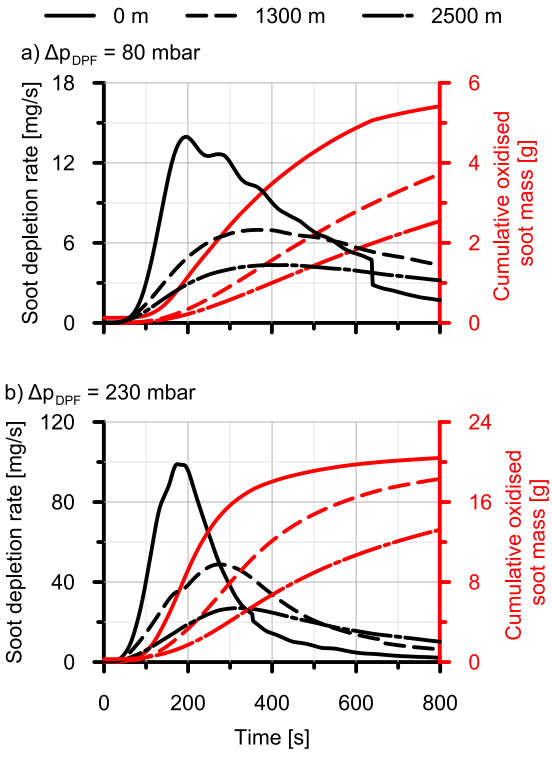

Fig. 6. Soot depletion rate and cumulative oxidised soot mass as a function of the altitude during active regeneration processes with initial DPF pressure drop (a) 80 mbar and (b) 230 mbar.

Fig. 7. Despite the lower O_2 partial pressures in altitude (Fig. 4(e)), the decrease of the substrate temperature, which was related to lower DPF inlet temperature (Fig. 4(c)), and the subsequent lower soot oxidation rate gave as a result higher oxygen surface coverage, which increased from 0.21 at sea level to 0.24–0.28 in altitude cases. Therefore, an enhancement of the oxidation rate was found from the O_2 point of view in altitude operation, but not enough to compensate the thermal conditions at the DPF inlet. This behaviour and the lack of influence of the mass transfer demonstrate that the thermal management was responsible for the regeneration process deterioration.

In order to quantify the coverage variation across the particulate layer, Fig. 8 shows the oxygen surface coverage at its inlet and outlet interfaces during active regenerations performed different altitudes and triggered at DPF pressure drops of 80 mbar and 230 mbar. Fig. 8(a) shows that the coverage barely varied from the inlet to the outlet regardless the altitude for 80 mbar in initial pressure drop. The low soot load corresponding to this case, and hence the small particulate layer thickness, contributed to almost constant oxygen concentration along the particulate layer, even during the maximum reactivity phase. In comparison, the higher temperature and soot depletion rate corresponding to the 230 mbar initial pressure drop case (Fig. 8(b)) made the coverage decrease with respect to the 80 mbar case. However, only small differences in oxygen surface coverage were found across the particulate layer again. In these cases, the coverage variation reached its maximum (9.4%) during the maximum reactivity phase at sea level ($\pm 200s$) and was progressively lowered as the altitude increased because of the soot depletion rate drop.

The deterioration of the regeneration process with altitude was also manifested in tailpipe CO and unburned HC emissions. As shown in Fig. 9(a), the CO emissions remained unaltered with respect to regular mode during the regeneration at sea-level. However, a huge increase at 1300 m (~ 3.5 times) and 2500 m (~ 4.5 times) was observed. Opposite to CO, the tailpipe unburned HC emission increase even took place during the regeneration at sea-level, reaching 8 times the regular

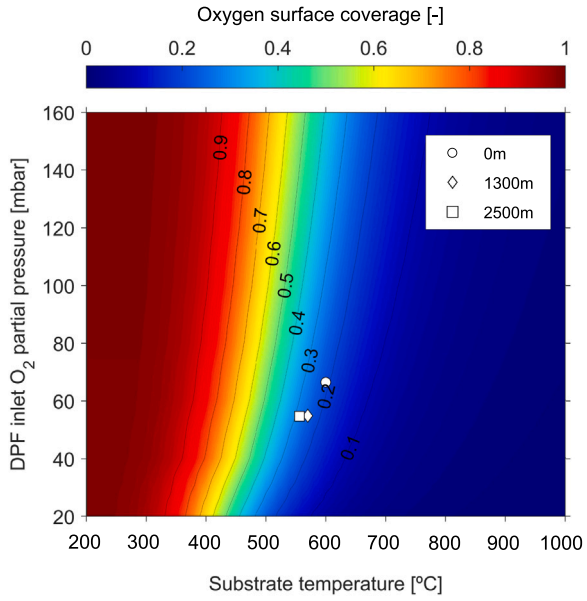

Fig. 7. Oxygen surface coverage as a function of the O_2 partial pressure and the substrate temperature.

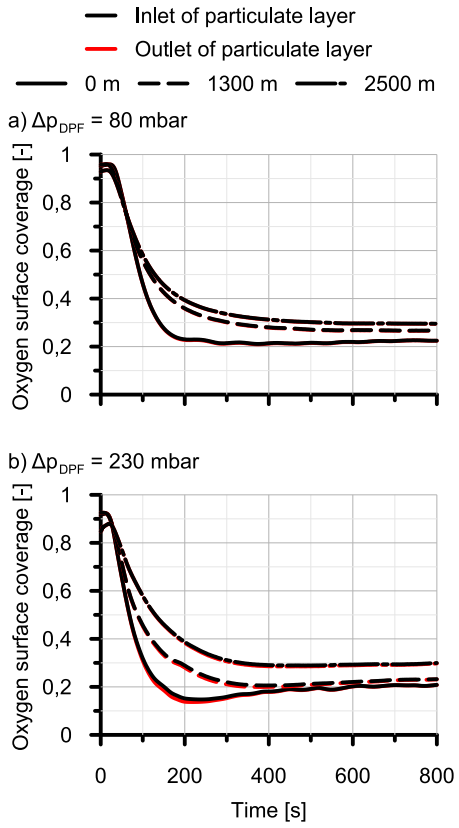

Fig. 8. Evolution of oxygen surface coverage as a function of altitude during active regeneration processes with initial DPF pressure drop of (a) 80 mbar and (b) 230 mbar.

mode emission, as observed in Fig. 9(b). As the altitude increased the unburned HC emission showed a linear increase in regeneration mode. The HC emission reached up to 35 times the corresponding to regular mode in the regenerations taking place at 2500 m. These trends in HC and CO emissions agreed with the post-injection efficiency reduction as the altitude increased, as shown in Fig. 4(d).

As regards tailpipe NO_x emissions, which are represented in Fig. 9(c), the regeneration strategy played a significant role due to its impact on the air management. Thus, the NO_x emissions increased in the regenerations performed at sea-level and 1300 m due to the LP-EGR rate reduction (Fig. 3(b)) with respect to regular mode. However, the LP-EGR rate was already very low in regular mode at 2500 m and its additional reduction in the regeneration mode was small. This slight reduction in LP-EGR rate at 2500 m combined with the lower equivalence ratio during the regeneration resulted in constant NO_x emissions for all pressure drop thresholds. Finally, Fig. 9(d) shows a decrease of the engine-out opacity when the regeneration mode was activated. This result was governed by the tendencies in LP-EGR rate and equivalence ratio. Despite the extremely low soot oxidation rates that were reached in altitude operation, the low opacity favoured the DPF balance point. It was delayed as the altitude increased due to the displacement of the equilibrium towards the soot oxidation caused by the low filtration rate.

4.1. VGT position impact on the soot oxidation rate

The trend to close the VGT as the altitude increases in regular mode has been already discussed to be negative for the engine and aftertreatment performance at partial loads [18]. The expected benefits from air mass flow increase because of the higher boost pressure are penalised by a high engine back-pressure. In fact, these operating conditions might be benefited by opener VGT with respect to sea-level in terms of both torque, BSFC and aftertreatment inlet temperature. In this context, the results shown in this work have also demonstrated that the VGT closing strategy as the altitude increases is also considered during the regeneration mode. As a result, poor soot oxidation performance is obtained at high altitude, even avoiding the regeneration completion. Evidence of the importance of VGT position optimisation to improve the thermal management of active filter regenerations is presented next.

Fig. 10 shows the engine performance sensitivity to the VGT position in regeneration mode. The engine was run in this mode at each altitude under steady-state conditions with clean DPF. Next, the VGT position was swept in a row. The fuel post-injection strategy and the LP-EGR valve position were kept the same as in the baseline tests, i.e. set by the series ECU calibration. Figs. 10(a) and (b) represent the torque and BSFC dependence on the VGT position at 1300 m and 2500 m. The VGT positions corresponding to baseline and those providing the maximum torque are highlighted. At the view of the results, an optimum VGT position exists in terms of torque maximisation (BSFC minimisation). The results also indicated that the higher the altitude the closer the VGT, as applied in series calibration. However, the optimised setting pointed out that the VGT position should be placed at 53% instead of 73% at 1300 m and at 73% instead of 100% at 2500 m. These new settings provided an increase in torque that exceeded 6.5% at 1300 m and almost 19% at 2500 m the baseline value. This result was due to, mainly, the reduction of the pumping work, as suggested by the huge reduction of the difference between the VGT inlet pressure and the boost pressure which are represented in Figs. 10(c) and (d). Despite these positive results, the boost pressure reduction brought by the optimum VGT position also produced the decrease of the air mass flow and the LP-EGR rate (Figs. 10(e) and (f)). Its impact on the emissions is analysed forwards.

Fig. 11(a) shows how extreme closed VGT positions contributed to increase the VGT inlet temperature, related to the high exhaust manifold pressure. However, an intermediate opening minimised the VGT inlet temperature. From this point on, higher VGT opening led again to higher VGT inlet temperature because of the gradual increase of the equivalence ratio. In parallel, the DPF inlet temperature, which is represented in Fig. 11(b), was also benefited by the VGT opening in the tested range due to an snowball effect bounded by the higher VGT inlet temperature and the lower VGT expansion ratio. These boundaries also improved the fuel post-injection efficiency, as plotted in Fig. 11(c). It

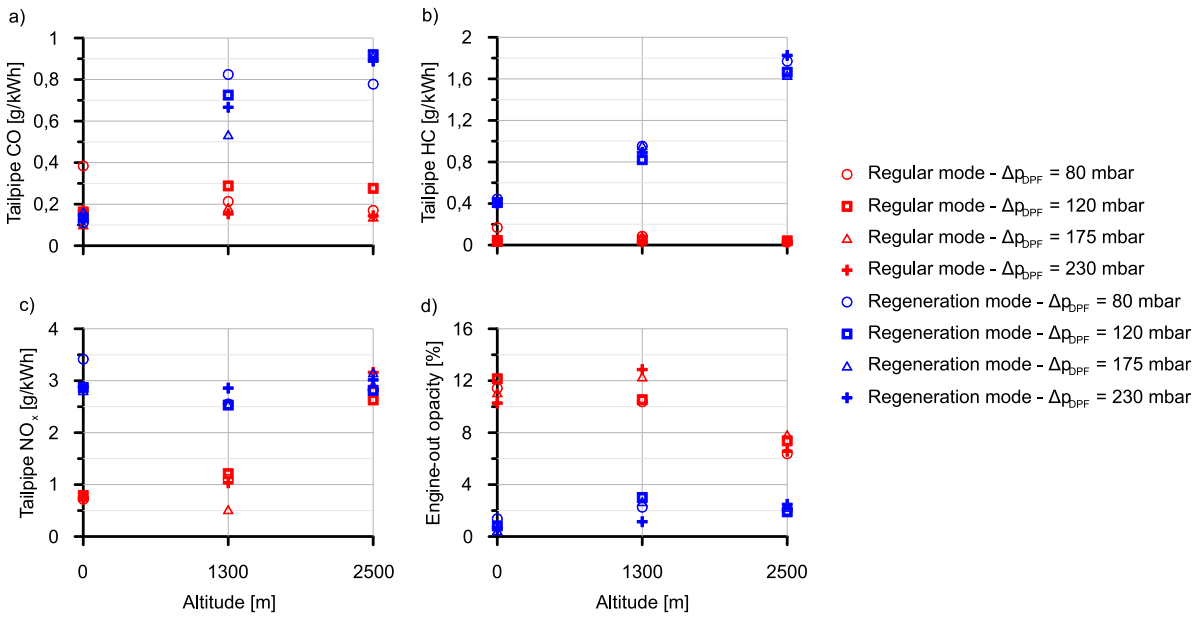

Fig. 9. Tailpipe gaseous pollutant emissions and engine-out opacity as a function of the engine operation mode, altitude and initial DPF pressure drop.

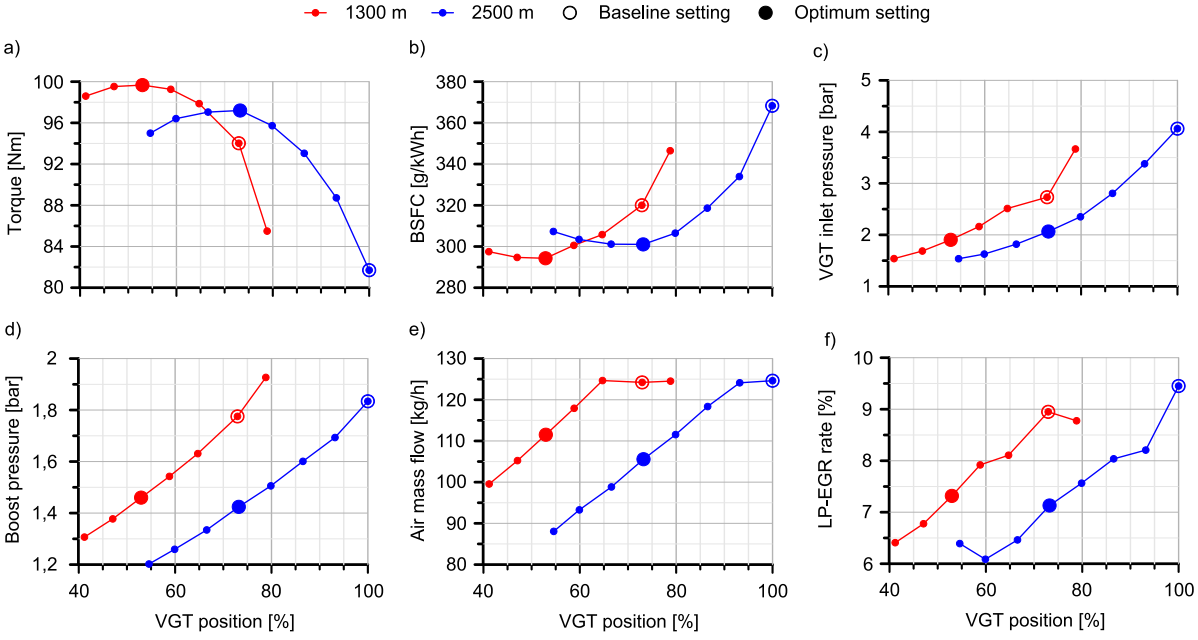

Fig. 10. Engine performance sensitivity to VGT position at 1300 m and 2500 m operating in regeneration mode.

was increased around 20 percentage points with respect to the baseline VGT position for both altitudes. In fact, the fuel post-injection efficiency reached values above the corresponding to sea-level, what resulted in higher DPF inlet temperature: 733.2°C and 718.3°C at 1300 m and 2500 m, respectively (Fig. 11(b)), compared to ~ 670°C at the sea level case shown in Fig. 4(c)).

Regarding other parameters influencing the soot oxidation rate, the DPF inlet O_2 partial pressure was lowered due to the opening of the VGT, as depicted in Fig. 11(d). The cause was the increase of the equivalence ratio produced by the air mass flow reduction. According to Fig. 7, this trend and the higher temperature across the DPF deteriorated the oxygen surface coverage under the new DPF boundary conditions. By contrast, the DPF residence time, which is presented in Fig. 11(e), was not very sensitive to the VGT position. Nevertheless, it showed a positive increasing tendency at both altitudes compared to the baseline VGT position. Nevertheless, it still remained below the corresponding counterpart at sea-level, which reached 0.0052 s (Fig. 4(f)).

With the boundaries set by the VGT position that maximised the torque at each altitude, in particular the higher temperature, the DPF regenerations were improved as shown in Fig. 12. The regenerations at sea-level are compared with those performed in altitude for the 120 mbar threshold of DPF pressure drop. A great increase of the soot depletion rate was obtained for altitude operation. As observed in Figs. 12(a) and (b), the proposed VGT position made the pressure drop profile converge to the trace corresponding to the baseline case at sea-level for both 1300 and 2500 m. The higher DPF inlet temperature required in altitude with respect to sea-level to reach this result was revealed as the most important parameter. However the oxygen surface coverage still impacted on the results. Although this parameter was proved in Fig. 7

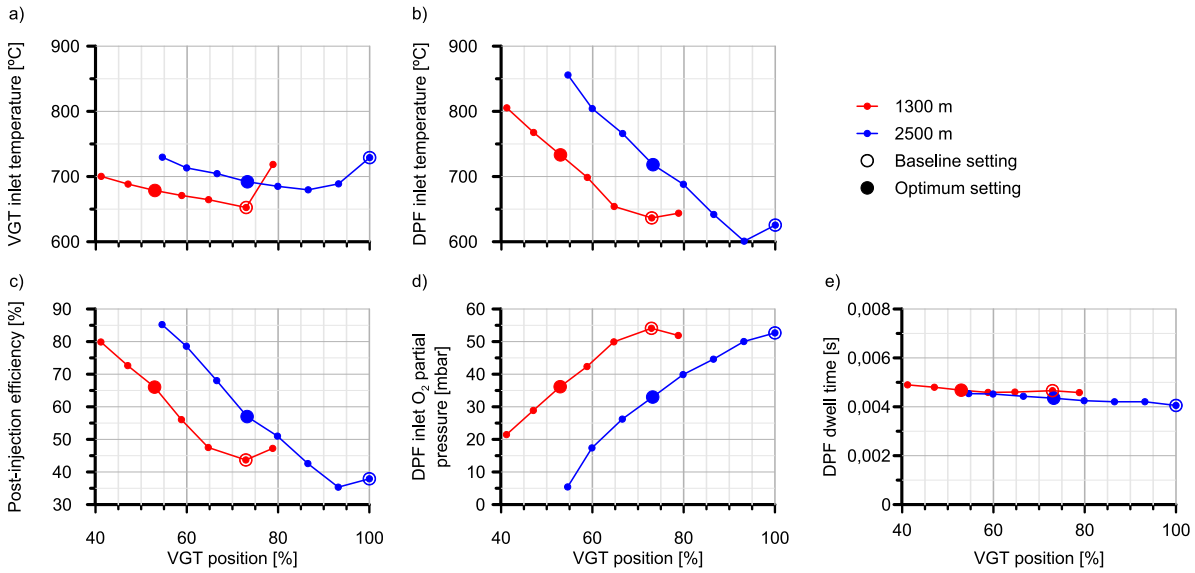

Fig. 11. Sensitivity to VGT position of VGT and DPF inlet temperatures, fuel post-injection efficiency, DPF inlet O_2 partial pressure and DPF residence time at 1300 m and 2500 m operating in regeneration mode.

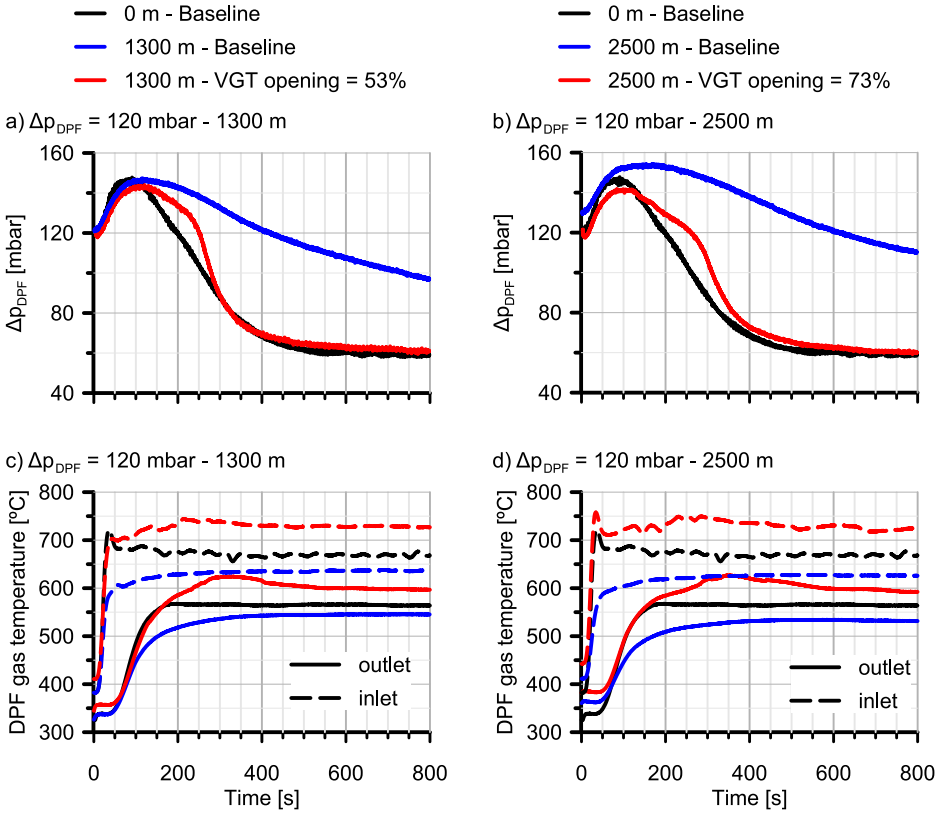

Fig. 12. Optimised active regenerations at high altitude to keep sea-level soot oxidation dynamics based on VGT position recalibration.

to be unable to compensate a low DPF inlet temperature, its decrease in the new regeneration strategy resulted in a snowball effect. The required temperature increase along with O_2 partial pressure decrease reduced the surface coverage what, in turn, led to the need of even higher exhaust temperature than the sea-level case to obtain a similar soot oxidation rate.

Finally, the new air management settings proposed to enhance the filter regeneration in altitude also affected the pollutant emissions. As summarised in Fig. 13, the opening of the VGT led to the decrease of the gaseous emissions in altitude operation. As a result, the tailpipe CO and unburned HC emissions at 1300 m (Euro 6 maximum altitude in RDE cycles) reached the same order of magnitude as the corresponding to the sea-level case during the regeneration. If the series calibration of the regeneration did not involve any issue to the fulfilment of Euro 6 CO and HC limits at least at sea-level, the proposed strategy to optimise the VGT actuation in this work should also contribute to avoiding issues at 1300 m. In parallel, the results corresponding to 2500 m evidenced that high altitude driving might impose more severe CO and HC emission

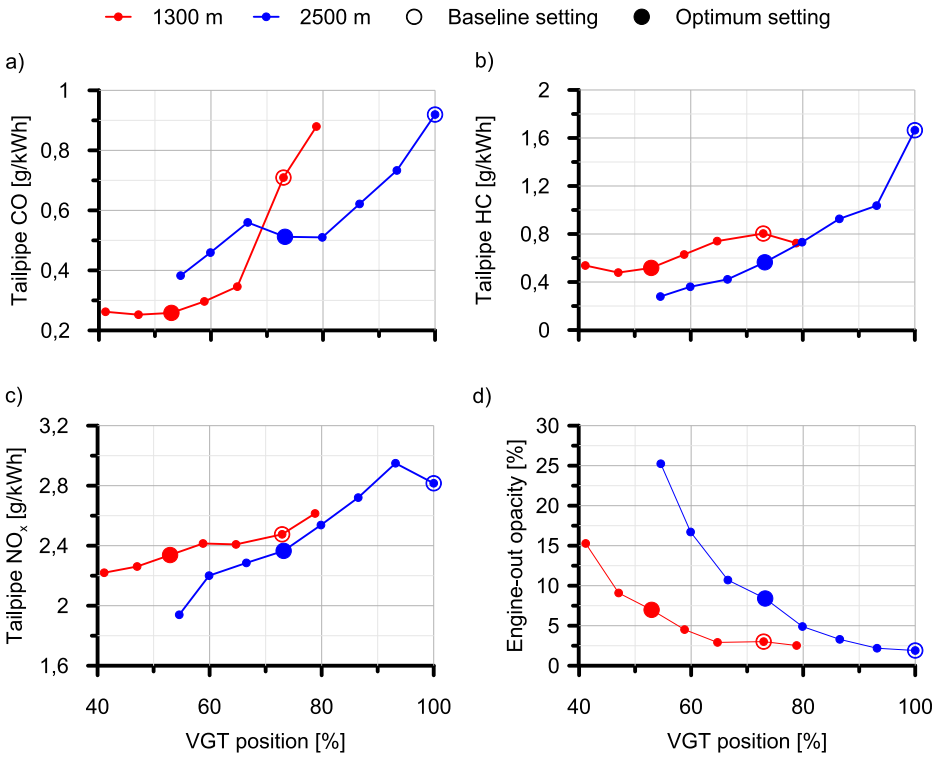

Fig. 13. VGT position influence on tailpipe gaseous pollutant emissions at 1300 m and 2500 m operating in regeneration mode.

control challenges, even after optimising the VGT control. With respect to the engine-out opacity, the new VGT positions produced an increase from ~ 2.5% to ~ 7.5% for both altitudes. This was conditioned by the gradual increase of the equivalence ratio as the VGT was opened. Despite this tendency, its value was still kept below the baseline one at sea-level conditions (~ 11%).

5. Summary and conclusions

This study has highlighted the importance of VGT actuation during active regeneration processes of wall-flow monoliths when operating at high driving altitudes. The experimental results obtained from series calibration in a Euro 6d-Temp Diesel engine evidenced a dramatic deterioration of the soot depletion rate. The balance point was reached in some tested cases, especially as the threshold soot mass load to trigger the active regeneration was low and the altitude increased. The VGT actuation was the main difference in engine control as a function of the altitude since the same fuel post-injection was applied by the series ECU calibration. The analysis of the experimental response along with the modelled results revealed that to close the VGT as the altitude increased failed during active regenerations. The main consequence was the reduction of the fuel post-injection efficiency, which was manifested by the decrease of the DPF inlet temperature. The modelled results demonstrated that this temperature governed the oxidation rate, although minor effects caused by the O_2 mass transfer and adsorption were also observed. In fact, the oxygen surface coverage was improved due to the lower temperature with respect to the sea-level case despite the also lower O_2 partial pressure in altitude operation. However, it did not compensate for the worsening of the exhaust thermal management.

In light of this baseline response, the optimisation of the air management, and in the VGT position, were identified as fundamental to improve the active regeneration strategy in altitude operation. Keeping constant the series ECU calibration as regards the fuel post-injection and LP-EGR rate, the opening of the VGT with respect to the series calibration setting provided relevant benefits in engine torque. Simultaneously, the higher VGT opening increased the exhaust temperature due to the combined effect of a higher equivalence ratio and lower VGT expansion ratio, thus improving the fuel post-injection efficiency. Consequently, the increase in soot depletion rate resulted in a DPF pressure drop along the regeneration equivalent to the one corresponding to the baseline operation at sea-level. The tailpipe pollutant emissions were also kept in the same order of magnitude as those at sea-level, and clearly decreased compared to altitude series calibration cases. Nevertheless, the regenerations performed in altitude required higher DPF inlet temperature than the sea-level cases to obtain the same results. This was due to the need to compensate for the lower residence time and oxygen surface coverage found at higher temperatures and equivalence ratios. Despite this constraint, the experimental results demonstrated that the penalties in the dynamics of active DPF regeneration related to altitude operation can be avoided provided that the VGT control strategy is adapted, which is in turn in synergy with engine performance and emissions enhancement.

CRediT authorship contribution statement

Pedro Piqueras: Funding acquisition, Project administration, Supervision, Conceptualization, Methodology, Writing – original draft. **Richard Burke:** Supervision, Validation, Writing – review & editing. **Enrique José Sanchis:** Resources, Formal analysis, Software, Data curation, Writing – original draft, Writing – review & editing. **Bárbara Diesel:** Visualization, Methodology, Software, Writing – original draft, Writing – review & editing.

Declaration of competing interest

The authors declare that they have no known competing financial interests or personal relationships that could have appeared to influence the work reported in this paper.

Acknowledgements

This research has been supported by Grant PID2020-114289RB-I00 funded by MCIN/AEI/10.13039/501100011033. Additionally, the PhD candidate Bárbara Diesel has been funded by a grant from the Government of Generalitat Valenciana and FSE (European Union) with reference ACIF/2018/109.

References

[1] Dowell PG, Akehurst S, Burke RD. Accuracy of diesel engine combustion metrics over the full range of engine operating conditions. J Eng Gas Turbine Power 2019;141(9):091005. http://dx.doi.org/10.1115/ICEF2018-9507.

[2] Delphi Technologies. Worldwide emission standards: Passenger cars and light duty vehicles 2019–2020. 2019.

[3] Szedlmayer M, Kweon C. Effect of altitude conditions on combustion and performance of a multi-cylinder turbocharged direct injection diesel engine. In: SAE technical paper 2016;2016-01-0742. http://dx.doi.org/10.4271/2016-01-0742.

[4] Bermúdez V, Serrano JR, Piqueras P, Gómez J, Bender S. Analysis of the role of altitude on diesel engine performance and emissions using an atmosphere simulator. Int J Engine Res 2017;18(1–2):105–17. http://dx.doi.org/10.1177/1468087416679569.

[5] Serrano JR, Piqueras P, Sanchis EJ, Diesel B. Analysis of the driving altitude and ambient temperature impact on the conversion efficiency of oxidation catalysts. Appl Sci 2021;11(3):1283. http://dx.doi.org/10.3390/app11031283.

[6] Wang X, Yin H, Ge Y, Yu L, Xu Z, Yu C, et al. On-vehicle emission measurement of a light-duty diesel van at various speeds at high altitude. Atmos Environ 2013;81:263–9. http://dx.doi.org/10.1016/j.atmosenv.2013.09.015.

[7] Giraldo H, Huertas JI. Real emissions, driving patterns and fuel consumption of in-use diesel buses operating at high altitude. Transp Res D 2019;77:21–36. http://dx.doi.org/10.1016/j.trd.2019.10.004.

[8] Ramos A, García-Contreras R, Armas O. Performance, combustion timing and emissions from a light duty vehicle at different altitudes fueled with animal fat biodiesel, GTL and diesel fuels. Appl Energy 2016;182:507–17. http://dx.doi.org/10.1016/j.apenergy.2016.08.159.

[9] Burke RD, Madamedon M, Williams R. Newly identified effects of injector nozzle fouling in diesel engines. Fuel 2020;278:118336. http://dx.doi.org/10.1016/j.fuel.2020.118336.

[10] Wang H, Ge Y, Hao L, Xu X, Tan J, Li J, Wu L, Yang J, Yang D, et al. The real driving emission characteristics of light-duty diesel vehicle at various altitudes. Atmos Environ 2018;191:126–31. http://dx.doi.org/10.1016/j.atmosenv.2018.07.060.

[11] Benjumea CP, Agudelo J, Agudelo A. Effect of altitude and palm oil biodiesel fuelling on the performance and combustion characteristics of a HSDI diesel engine. Fuel 2009;88:725–31. http://dx.doi.org/10.1016/j.fuel.2008.10.011.

[12] Soltani S, Andersson R, Andersson B. The effect of exhaust gas composition on the kinetics of soot oxidation and diesel particulate filter regeneration. Fuel 2018;220:453–63. http://dx.doi.org/10.1016/j.fuel.2018.02.037.

[13] Serrano JR, Piqueras P, Sanchis EJ, Diesel B. A modelling tool for engine and exhaust aftertreatment performance analysis in altitude operation. Results Eng 2019;4:100054. http://dx.doi.org/10.1016/j.rineng.2019.100054.

[14] Serrano JR, Climent H, Piqueras P, Angiolini E. Analysis of fluid-dynamic guidelines in diesel particulate filter sizing for fuel consumption reduction in post-turbo and pre-turbo placement. Appl Energy 2014;132:507–23. http://dx.doi.org/10.1016/j.apenergy.2014.07.043.

[15] Lapuerta M, Rodríguez-Fernández J, Oliva F. Effect of soot accumulation in a diesel particle filter on the combustion process and gaseous emissions. Energy 2012;47:543–53. http://dx.doi.org/10.1016/j.energy.2012.09.054.

[16] Beatrice C, Iorio SDi, Guido C, Napolitano P. Detailed characterization of particulate emissions of an automotive catalyzed DPF using actual regeneration strategies. Exp Therm Fluid Sci 2012;39:45–53. http://dx.doi.org/10.1016/j.expthermflusci.2012.01.005.

[17] Thompson AT. The effect of altitude on turbocharger performance parameters for heavy duty diesel engines: experiments and Gt-power modeling. (Ph.D. thesis), Colorado State University; 2014.

[18] Bermúdez V, Serrano JR, Piqueras P, Diesel B. Fuel consumption and aftertreatment thermal management synergy in compression ignition engines at variable altitude and ambient temperature. Int J Engine Res 2021. http://dx.doi.org/10.1177/14680874211035015, Online First.

[19] Burke RD, Burke KA, Chappell EC, Gee M, William R. A novel use of multivariate statistics to diagnose test-to-test variation in complex measurement systems. Measurement 2018;130:467–81. http://dx.doi.org/10.1016/j.measurement.2018.07.059.

[20] Serrano JR, Piqueras P, De la Morena J, Sanchis EJ. Late fuel post-injection influence on the dynamics and efficiency of wall-flow particulate filters regeneration. Appl Sci 2019;9(24):5384. http://dx.doi.org/10.3390/app9245384.

[21] He Q, Guo Q, Umeki K, Ding L, Wang F, Yu G. Soot formation during biomass gasification: A critical review. Renew Sust Energ Rev 2021;139:110710. http://dx.doi.org/10.1016/j.rser.2021.110710.

[22] Xie Y, Zuo Q, Wang M, Wei K, Zhang B, Chen W, et al. Effects analysis on soot combustion performance enhancement of an improved catalytic gasoline particulate filter regeneration system with electric heating. Fuel 2021;290:119975. http://dx.doi.org/10.1016/j.fuel.2020.119975.

[23] Wang X, Li S, Adeosun A, Li Y, Vujanović M, Tan H, et al. Effect of potassium-doping and oxygen concentration on soot oxidation in O_2/CO_2 atmosphere: A kinetics study by thermogravimetric analysis. Energy Convers Manag 2017;149:686–97. http://dx.doi.org/10.1016/j.enconman.2017.01.003.

[24] Du J, Su L, Zhang D, Jia C, Yuan Y. Experimental investigation into the pore structure and oxidation activity of biodiesel soot. Fuel 2022;310:122316. http://dx.doi.org/10.1016/j.fuel.2021.122316.

[25] Prasad R, Singh SV. A review on catalytic oxidation of soot emitted from diesel fuelled engines. J Environ Chem Eng 2020;8(4):103945. http://dx.doi.org/10.1016/j.jece.2020.103945.

[26] Macián V, Serrano JR, Piqueras P, Sanchis EJ. Internal pore diffusion and adsorption impact on the soot oxidation in wall-flow particulate filters. Energy 2019;179:407–21. http://dx.doi.org/10.1016/j.energy.2019.04.200.

[27] Deng Y, Zheng W, Jiaqiang E, Zhang B, Zhao X, Zuo Q, et al. Influence of geometric characteristics of a diesel particulate filter on its behavior in equilibrium state. Appl Therm Eng 2017;123:61–73. http://dx.doi.org/10.1016/j.applthermaleng.2017.05.071.

[28] Jaramillo IC, Gaddam CK, Wal RLVander, Lighty JS. Effect of nanostructure, oxidative pressure and extent of oxidation on model carbon reactivity. Combust Flame 2015;162(5):1848–56. http://dx.doi.org/10.1016/j.combustflame.2014.12.006.

[29] Hurt RH, Haynes BS. On the origin of power-law kinetics in carbon oxidation. Proc Combust Inst 2005;30(2):2161–8. http://dx.doi.org/10.1016/j.proci.2004.08.131.

[30] Piqueras P, Sanchis EJ, Herreros JM, Tsolakis A. Evaluating the oxidation kinetic parameters of gasoline direct injection soot from thermogravimetric analysis experiments. Chem Eng Sci 2021;234:116437. http://dx.doi.org/10.1016/j.ces.2021.116437.

[31] Kalogirou M, Samaras Z. A thermogravimetic kinetic study of uncatalyzed diesel soot oxidation. J Therm Anal Calorim 2009;98(1):215–24. http://dx.doi.org/10.1007/s10973-009-0110-8.

[32] Zouaoui N, Labaki M, Jeguirim M. Diesel soot oxidation by nitrogen dioxide, oxygen and water under engine exhaust conditions: kinetics data related to the reaction mechanism. C R Chim 2014;17(7–8):672–80. http://dx.doi.org/10.1016/j.crci.2013.09.004.

[33] Kim JH, Kim MY, Kim HG. $NO_2 - assisted$ Soot regeneration behavior in a diesel particulate filter with heavy-duty diesel exhaust gases. Numer Heat Transf A Appl 2010;58(9):725–39. http://dx.doi.org/10.1080/10407782.2010.523293.

[34] Desantes JM, Galindo J, Payri F, Piqueras P, Serrano JR. Device for atmosphere conditioning for testing combustion engines, and associated method and use, Patent WO 2015/110683 A1; 2015.

[35] Desantes JM, Galindo J, Payri F, Piqueras P, Serrano JR. Device for conditioning the atmosphere in test of alternative internal combustion engines, method and use of said device, Patent WO 2016/116642 A1; 2016.

[36] Galindo J, Serrano JR, Piqueras P, Gómez J. Description and performance analysis of a flow test rig to simulate altitude pressure variation for internal combustion engines testing. SAE Int J Engines 2014;4(7):1686–96. http://dx.doi.org/10.4271/2014-01-2582.

[37] Broatch A, Bermúdez V, Serrano JR, Tabet R, Gómez J, Bender S. Analysis of passenger car turbocharged diesel engines performance when tested at altitude and of the altitude simulator device used. J Eng Gas Turbines Power 2019;141(8):081017. http://dx.doi.org/10.1115/1.4043395.

[38] Payri F, Broatch A, Serrano JR, Piqueras P. Experimental-theoretical methodology for determination of inertial pressure drop distribution and pore structure properties in wall-flow diesel particulate filters (DPFs). Energy 2011;36(12):6731–44. http://dx.doi.org/10.1016/j.energy.2011.10.033.

[39] Wu Y, Wang P, Farhan S, Yi J, Lei L. Effect of post-injection on combustion and exhaust emissions in DI diesel engine. Fuel 2019;258:116131. http://dx.doi.org/10.1016/j.fuel.2019.116131.

[40] Meng Z, Chen C, Li J, Fang J, Tan J, Qin Y, et al. Particle emission characteristics of DPF regeneration from DPF regeneration bench and diesel engine bench measurements. Fuel 2020;262:116589. http://dx.doi.org/10.1016/j.fuel.2019.116589.

[41] Payri F, Arnau FJ, Piqueras P, Ruiz MJ. Lumped approach for flow-through and wall-flow monolithic modelling for real-time automotive applications. In: SAE technical paper 2018. 2018-01-0954, http://dx.doi.org/10.4271/2018-01-0954.

[42] Serrano JR, Arnau FJ, Piqueras P, Afonso Ó García. Packed bed of spherical particles approach for pressure drop prediction in wall-flow DPFs (diesel particulate filters) under soot loading conditions. Energy 2013;58:644–54. http://dx.doi.org/10.1016/j.energy.2013.05.051.

[43] Galindo J, Serrano JR, Piqueras P, Afonso Ó García. Heat transfer modelling in honeycomb wall-flow diesel particulate filters. Energy 2012;43:201–13. http://dx.doi.org/10.1016/j.energy.2012.04.044.

[44] Serrano JR, Climent H, Piqueras P, Angiolini E. Filtration modelling in wall-flow particulate filters of low soot penetration thickness. Energy 2016;112:883–98. http://dx.doi.org/10.1016/j.energy.2016.06.121.

[45] Abián M, Martín C, Nogueras P, Sánchez-Valdepeñas J, Rodríguez-Fernández J, Lapuerta M, et al. Interaction of diesel engine soot with NO_2 and O_2 at diesel exhaust conditions. Effect of fuel and engine operation mode. Fuel 2018;212:455–61. http://dx.doi.org/10.1016/j.fuel.2017.10.025.

[46] Jeguirim M, Tschamber V, Brilhac JF, Ehrburger P. Oxidation mechanism of carbon black by NO_2: effect of water vapour. Fuel 2005;84(14):1949–56. http://dx.doi.org/10.1016/j.fuel.2005.03.026.

[47] Dardiotis CK, Haralampous OA, Koltsakis GC. Catalytic oxidation in wall-flow reactors with zoned coating. Chem Eng Sci 2008;63(4):1142–53. http://dx.doi.org/10.1016/J.CES.2007.11.012.

[48] Zhao X, Jiaqiang E, Liao G, Zhang F, Chen J, Deng Y. Numerical simulation study on soot continuous regeneration combustion model of diesel particulate filter under exhaust gas heavy load. Fuel 2021;290:119795. http://dx.doi.org/10.1016/j.fuel.2020.119795.

[49] Messerer A, Niessner R, Pöschl U. Comprehensive kinetic characterization of the oxidation and gasification of model and real diesel soot by nitrogen oxides and oxygen under engine exhaust conditions: Measurement, Langmuir-Hinshelwood, and Arrhenius parameters. Carbon 2006;44:307–24. http://dx.doi.org/10.1016/j.carbon.2005.07.017.

[50] Stanmore BR, Tschamber V, Brilhac JFOxidation of carbon by NOx. With particular reference to NO_2 and N_2O. Fuel 2008;87(2):131–46. http://dx.doi.org/10.1016/j.fuel.2007.04.012.

[51] Essenhigh RH. Influence of initial particle density on the reaction mode of porous carbon particles. Combust Flame 1994;99:269–79. http://dx.doi.org/10.1016/0010-2180(94)90131-7.

[52] Lee KJ, Han IH, Choi KH. Oxygen chemisorption on microporous carbons: an analysis of experimental data. Korean J Chem Eng 1995;12:228–35. http://dx.doi.org/10.1007/BF02705651.

[53] Kalberer M, Ammann M, Gaggeler HW, Baltensperger U. Adsorption of NO_2 on carbon aerosol particles in the low ppb range. Atmos Environ 1999;33:2815–22. http://dx.doi.org/10.1016/S1352-2310(98)00390-2.